Two Degree of Freedom Hamiltonian Systems in Chemical Reaction Dynamics – A Phase Space Analysis

Sam Spedding

Summer 2020

Contents

1 Introduction

In this report we further the investigation into the phase space analysis of two degree of freedom Hamiltonian systems in the field of chemical reaction dynamics. We start by studying, the De Leon Berne system, a benchmark system that has been well studied over the past half century, with the goal of gaining an understanding of the reaction phenomena that can be applied to more complicated systems. We then move onto one of these more complex systems: the Gezelter-Miller three-well potential.

In [1], the topic of normally hyperbolic invariant manifolds, or NHIMs, and dividing surfaces is explained, and it is these concepts that will be the basis for gaining an understanding of these potentials.

2 The De Leon Berne Hamiltonian

In this section we look at an example two-degree-of-freedom non-linear coupled system from De Leon and Berne [2]. The system is a simplified model for butane isomerisation in which there is an oscillatory coordinate x, and a reactive coordinate y. The energy Hamiltonian is given by

$$\mathcal{H}(x, y, p_x, p_y) = \frac{p_x^2}{2m_x} + \frac{p_y^2}{2m_y} + V(x, y) \tag{1}$$

where the potential energy function consists of

- a double well potential in the y coordinate

  $$V_{\mathrm{DW}}(y) = \frac{\mathcal{V}^\ddagger}{y_w^4} y^2(y^2 - 2y_w^2) + \epsilon_s$$

  where parameters $V^\ddagger$, y_w and ϵ_s are the uncoupled well depth, well location and energy of the barrier respectively;

- a Morse oscillator in the x coordinate

  $$V_{\mathrm{M}}(x) = D_x(1 - e^{-\lambda x})^2$$

  where D_x and λ are the dissociation energy and range of the Morse potential respectively;

- and a coupling term

  $$V_{\mathrm{DWM}}(x, y) = \frac{\mathcal{V}^\ddagger}{y_w^4} y^2(y^2 - 2y_w^2) \left[e^{-\zeta\lambda x} - 1\right]$$

  where the parameter ζ controls the strength of the coupling.

Putting it all together the potential energy is

$$\begin{aligned} V(x, y) &= V_{\mathrm{DW}}(x, y) + V_{\mathrm{M}}(x, y) + V_{\mathrm{DWM}}(x, y) \\ &= D_x(1 - e^{-\lambda x})^2 + \frac{\mathcal{V}^\ddagger}{y_w^4} y^2(y^2 - 2y_w^2)e^{-\zeta\lambda x} + \epsilon_s \end{aligned} \tag{2}$$

In the calculations that follow we fix the parameters $m_x = m_y = 8$, $D_x = 10$, and $\mathcal{V}^\ddagger = \epsilon_s = 1$ to be in line with the literature, and we shall vary λ and ζ.

Hamilton's equations for this system are given by

$$\begin{aligned} \dot{x} &= \frac{\partial \mathcal{H}}{\partial p_x} = \frac{p_x}{m_x} \\ \dot{y} &= \frac{\partial \mathcal{H}}{\partial p_y} = \frac{p_y}{m_y} \\ \dot{p_x} &= -\frac{\partial \mathcal{H}}{\partial x} = 2D_x\lambda e^{-\lambda x}(e^{-\lambda x} - 1) + \frac{\mathcal{V}^\ddagger}{y_w^4} y^2(y^2 - 2y_w^2)\zeta\lambda e^{-\zeta\lambda x} \\ \dot{p_y} &= -\frac{\partial \mathcal{H}}{\partial y} = -4\frac{\mathcal{V}^\ddagger}{y_w^4} y(y^2 - y_w^2)e^{-\zeta\lambda x} \end{aligned} \tag{3}$$

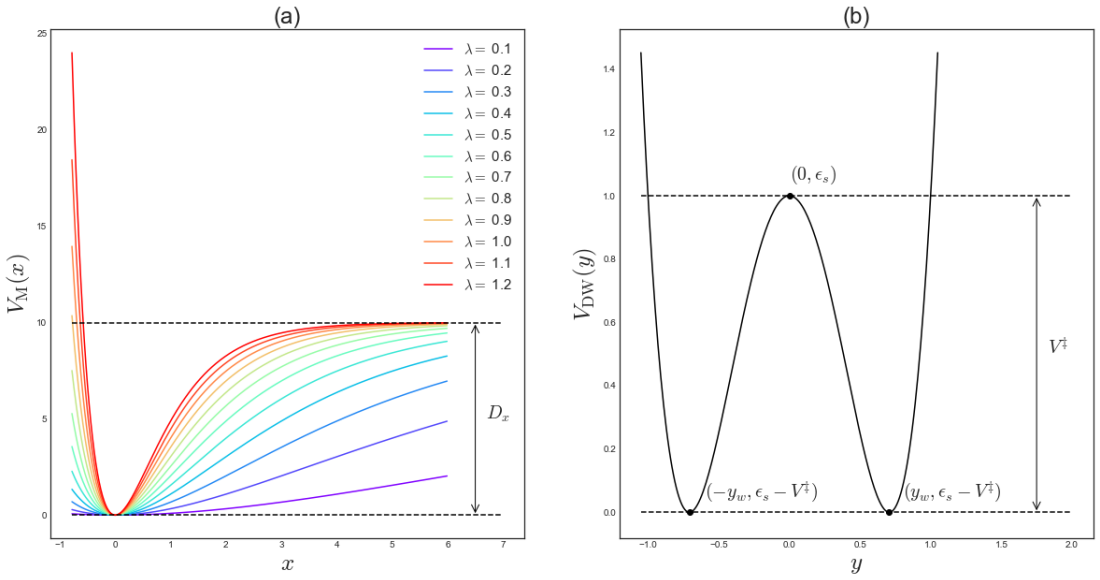

Figure 1: (a): Plot of morse oscillator for varying λ. x coordinate dissociates (becomes unbounded) for energies higher than $D_x + \epsilon_s$; (b): double well potential plot showing uncoupled well depth $V^{\ddagger}$, well positions $\pm y_w$ and saddle energy ϵ_s.

2.1 Poincaré Surfaces of Section for the De Leon Berne system

Often the first port of call for understanding the behaviour of nonlinear Hamiltonian systems is the Poincare section, which reduces the dimensionality of some of the characteristics of the system to something we can more easily visualise. With two degrees of freedom, the phase space is four-dimensional. However our retinas and computer monitors are two-dimensional, meaning visualisation of the phase space necessarily requires some projection onto lower-dimensional surfaces. First we may reduce the dimension to three by fixing the total energy of the system, i.e. considering the invariant manifold of constant energy. Then to reduce by a further dimension, there are a couple of ways to define a two-dimensional section of this energy surface, namely:

- to fix a momentum co-ordinate and consider an array of points in configuration space, (x, y), and to rearrange for the other momentum coordinate in terms of the total energy; or
- to fix a position co-ordinate and consider pairs of conjugate position and momentum co-ordinates (x, p_x) or (y, p_y), and to rearrange for the other momentum coordinate in terms of the total energy.

Once we've calculated an array of points on our section that have the same energy, we use these points as initial conditions for our system to generate an ensemble of trajectories, which are obtained by numerically integrating the system over a sufficiently long time period. The plot of all the points on the section through which the trajectories recross the same section at a later time is called a Poincaré (surface of) section.

Figures 2 to 4 show Poincaré sections for the De Leon Berne system with varying values for λ, ζ and the total energy.

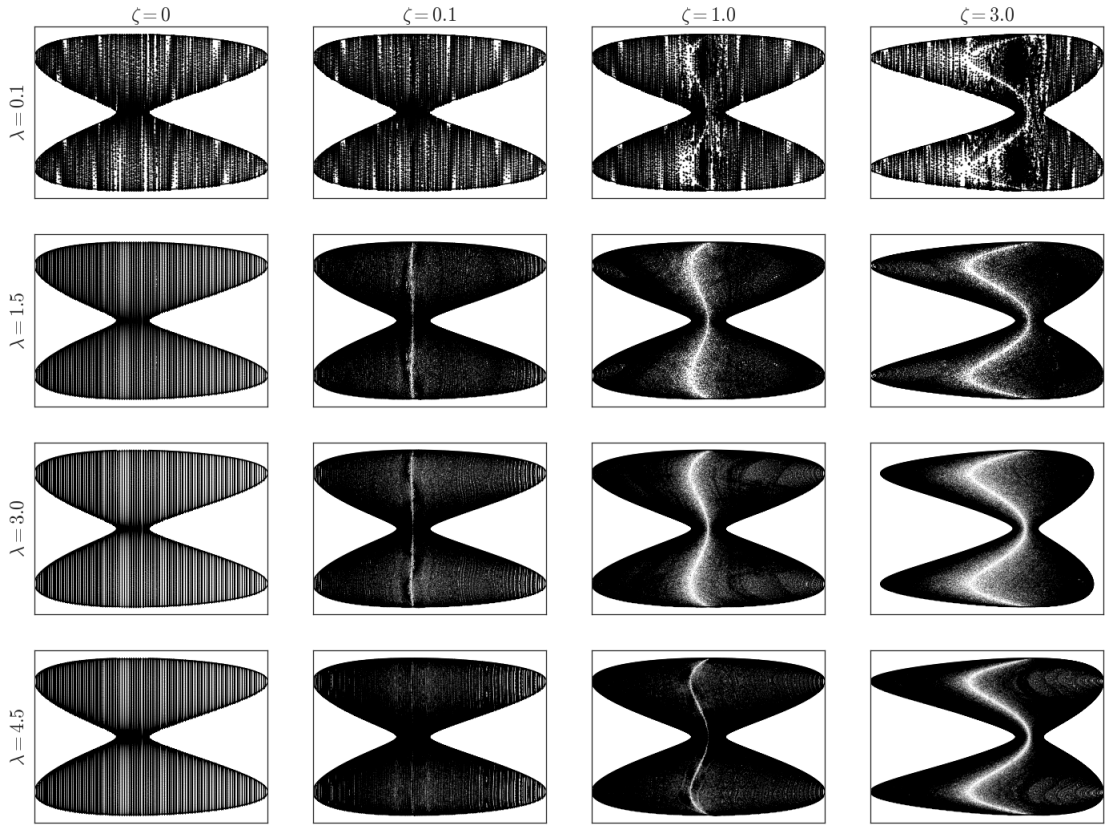

Figure 2: Poincaré sections $p_x = 0$ in configuration space for varying values of λ and ζ. Total energy $E = 1.02$. Vertcial lines seen in sections for low values of ζ and λ indicate uncoupled behaviour in which the x coordinate oscillates independently of the y coordinate. The x coordinate of the vertical lines correspond to the turning points of the Morse oscillator . The lines that pass through the bottleneck correspond to trajectories that pass back and forth across the barrier, while those that don't correspond to trajectories forever trapped in either well [2]. As λ and ζ are increased, these structures start to decay, as trapped trajectories become able to cross over, and crossing trajectories become trapped. The distinctive lighter regions shaped like waves in $\zeta = 1$ and $\zeta = 3$ pass through the centre in each well and correspond to regions in which the x-coordinate is never stationary.

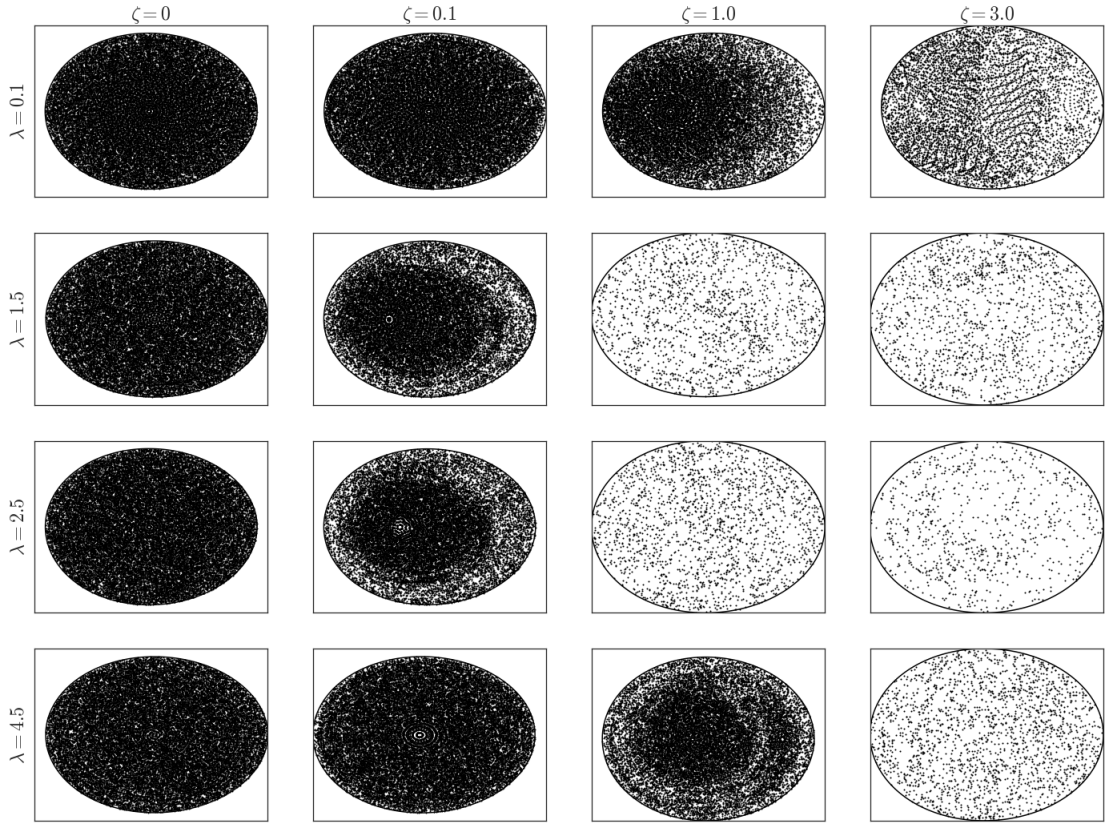

Figure 3: Poincaré sections $y = 0$ in (x, p_x) space for varying values of λ and ζ. Total energy $E = 1.02$.

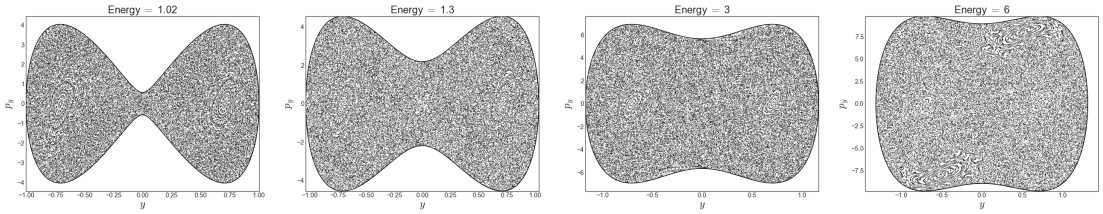

Figure 4: Poincaré sections $x = 0$ in (y, p_y) space for varying total energy values. $\lambda = 1.5$, $\zeta = 1$.

2.2 Dividing Surface for the De Leon Berne System

In this section we study the notion of a dividing surface (DS), which in the context of Hamiltonian systems may be described as a surface embedded in the phase space through which all reacting trajectories must cross. Some key features of a dividing surface are

- it is embedded within the energy surface, i.e. we must consider the diving surface for a

fixed value of the energy E (we can varying the total energy to get a different diving surface for that new energy level);

- all reacting trajectories must cross the diving surface, i.e. it is the surface in phase space that divides reactant and product states;
- it has a 'local no recrossing' property, i.e. over sufficiently small timescales, a trajectory can only cross the dividing surface once. In order to recross, it must spend a sufficiently long period of time inside the well it has crossed over into.

For more details, c.f. [1].

In the De Leon Berne model, the reaction takes place when the reaction coordinate, y, changes sign. Thus all reacting trajectories must pass through this plane, so we define a DS by the intersection with $y = 0$ and the energy surface at energy level E. From a phase space perspective, the DS can be written in terms of the remaining state variables and the energy:

$$D_x(1 - e^{-\lambda x})^2 + \epsilon_s + \frac{p_x^2}{2m_x} + \frac{p_y^2}{2m_y} = E, \tag{4}$$

which is isomorphic to a two-sphere embedded in the four-dimensional phase space. The intersection between the DS and the plane $p_y = 0$ forms the equator of the sphere and is given by

$$D_x(1 - e^{-\lambda x})^2 + \epsilon_s + \frac{p_x^2}{2m_x} = E. \tag{5}$$

Equation (5) describes an unstable periodic orbit (UPO), since at $y = 0$, p_y also remains zero, meaning only the Morse oscillator in the x variable (which has Lyapunov-stable periodic orbits) remains, while deviating away from $y = 0$ gives a deviation in p_y of the same sign, thus causing instability. We see that along the coordinates (y, p_y), which are normal to the UPO, the dynamics are of saddle-type behaviour, which makes the orbit (which is also a manifold) a NHIM.

The procedure for sampling the DS as described in [4] may be applied to this particular model analytically as follows:

1. The UPO is given by equation (5).
2. Projection of the UPO onto configuration space gives us

$$(1 - e^{-\lambda x})^2 \leq \frac{E - \epsilon_s}{D_x} = \kappa^2 \tag{6}$$

   (defining $\kappa := \sqrt{(E - \epsilon_s)/D_x}$), which is a one-dimensional line segment along the x-axis for $x_{\min} \leq x \leq x_{\max}$. We can calculate

$$\begin{aligned} x_{\min} &= -\frac{1}{\lambda} \log(1 + \kappa) \\ x_{\max} &= -\frac{1}{\lambda} \log(1 - \kappa). \end{aligned} \tag{7}$$

3. Next we select N points on the configuration space projection of the UPO, (x_i, y_i), $1 \leq i \leq N$. In this case $x_{\min} \leq x_i \leq x_{\max}$ and $y_i = 0$ for each i. Then for each (x_i, y_i), we can

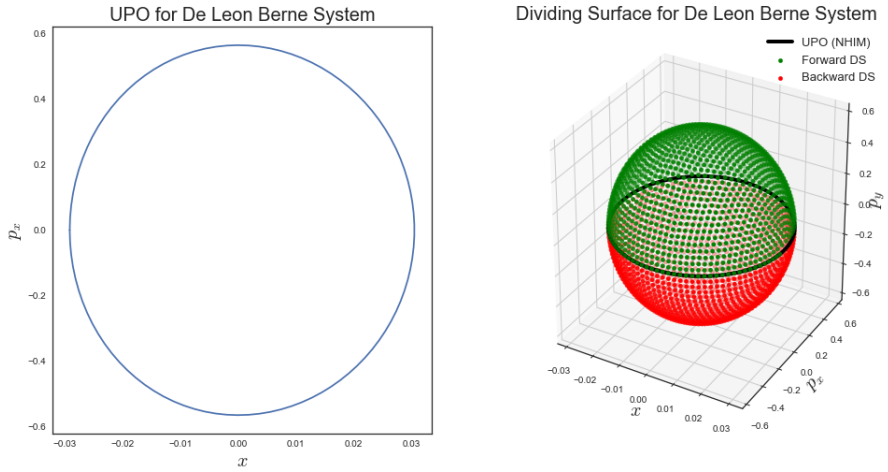

Figure 5: UPO and DS for the De Leon Berne system at total energy $E = 1.02$.

use equation (1) to obtain

$$\frac{p_x^2}{2m_x} + \frac{p_y^2}{2m_y} = E - V(x_i, y_i), \tag{8}$$

which is the equation for an ellipse in momentum space. This may be sampled by letting

$$\begin{aligned} p_x &= \sqrt{2m_x \left(E - V(x_i, y_i)\right)} \cos\theta_j \\ p_y &= \sqrt{2m_y \left(E - V(x_i, y_i)\right)} \sin\theta_j \end{aligned} \tag{9}$$

where θ_j, $1 \leq j \leq M$ for some M, are uniformly spaced in the interval $[0, 2\pi)$. The points for which $\theta_j \in (0, \pi)$ (and hence $p_y > 0$) make up the forward DS and points with $\theta_j \in (\pi, 2\pi)$ are on the backward DS.

2.2.1 Sampling the DS uniformly

With the method described in step 3, the points are not sampled uniformly across the DS if we choose M to be the same for each (x_i, y_i); the points will be more densely packed around the values for which the radii of the ellipse are smaller, i.e. constant M favours points with smaller kinetic energy.

In order to sample the DS uniformly, we let the number of values for θ_j depend on the radii of the ellipse. What follows is a method that works for when $m_x = m_y = m$ and the ellipses are circles:

As before, select N points on the UPO in configuration space, (x_i, y_i), $1 \leq i \leq N$. Now calculate the maximum radius of all the circles

$$p_{\max} := \max_{1 \leq i \leq N} \left\{ \sqrt{2m \left(E - V(x_i, y_i)\right)} \right\}.$$

Then for each (x_i, y_i), select M_i uniformly spaced values of $\theta \in [0, \pi)$, where

$$M_i = \left\lfloor \frac{N\sqrt{2m\left(E - V(x_i, y_i)\right)}}{p_{\max}} + \frac{1}{2} \right\rfloor,$$

which is the value of N scaled by the ratio of the radius at position i and the maximum radius, rounded to the nearest integer.

2.3 Linearisation and Quadratic Normal Form

It is often helpful in the study of non-linear dynamical systems to consider the linearisation of the system centred about a point of interest: in this case, the saddle at the origin. Linearising the vector field generated by Hamilton's equations (3) amounts to expanding the Hamiltonian up to quadratic terms. We Taylor expand about the saddle point, which is located at $x = y = 0$. Note that the kinetic energy part of the Hamiltonian is already quadratic, so we just need to expand the potential:

$$V(x, y) = D_x\lambda^2 x^2 - 2\frac{\mathcal{V}^\ddagger}{y_w^2}y^2 + \epsilon_s + \mathcal{O}((x + y)^3). \tag{10}$$

This gives us the quadratic normal form

$$\mathcal{H}_{\text{quadratic}} = \frac{p_x^2}{2m_x} + \frac{p_y^2}{2m_y} + D_x\lambda^2 x^2 - \frac{2\mathcal{V}^\ddagger}{y_w^2}y^2 + \epsilon_s. \tag{11}$$

The system is locally uncoupled, with the coupling constant ζ only multiplying cubic terms and higher. The linearised system then becomes

$$\frac{\mathrm{d}}{\mathrm{d}t}\begin{pmatrix} x \\ p_x \\ y \\ p_y \end{pmatrix} = \begin{pmatrix} p_x/m_x \\ -2D_x\lambda^2 x \\ p_y/m_y \\ 4\mathcal{V}^\ddagger y/y_w^2 \end{pmatrix} = \begin{pmatrix} 0 & 1/m_x & 0 & 0 \\ -2D_x\lambda^2 & 0 & 0 & 0 \\ 0 & 0 & 0 & 1/m_y \\ 0 & 0 & 4\mathcal{V}^\ddagger/y_w^2 & 0 \end{pmatrix}\begin{pmatrix} x \\ p_y \\ y \\ p_y \end{pmatrix} \tag{12}$$

which has analytic solution

$$\begin{aligned}
x(t) &= x(0)\cos\left(\lambda\sqrt{\frac{2D_x}{m_x}}t\right) + p_x(0)\frac{1}{\lambda\sqrt{2D_x m_x}}\sin\left(\lambda\sqrt{\frac{2D_x}{m_x}}t\right), \\
p_x(t) &= p_x(0)\cos\left(\lambda\sqrt{\frac{2D_x}{m_x}}t\right) - x(0)\lambda\sqrt{2D_x m_x}\sin\left(\lambda\sqrt{\frac{2D_x}{m_x}}t\right), \\
y(t) &= y(0)\cosh\left(\frac{2}{y_w}\sqrt{\frac{\mathcal{V}^\ddagger}{m_y}}t\right) + p_y(0)\frac{y_w}{2\sqrt{\mathcal{V}^\ddagger m_y}}\sinh\left(\frac{2}{y_w}\sqrt{\frac{\mathcal{V}^\ddagger}{m_y}}t\right), \\
p_y(t) &= p_y(0)\cosh\left(\frac{2}{y_w}\sqrt{\frac{\mathcal{V}^\ddagger}{m_y}}t\right) + y(0)\frac{2\sqrt{\mathcal{V}^\ddagger m_y}}{y_w}\sinh\left(\frac{2}{y_w}\sqrt{\frac{\mathcal{V}^\ddagger}{m_y}}t\right).
\end{aligned} \tag{13}$$

It is clear from the solution of the linearised system that the origin is an index-1 saddle equilibrium point, with the (x, p_x) coordinates behaving oscillatory for small deviations from the origin and the (y, p_y) coordinates behaving hyperbolically.

2.3.1 Quadratic Normal Form of the Hamiltonian

The next goal is to obtain a Hamiltonian in a canonical form for the linearised system described above, i.e. one that has the form

$$H_{\text{canonical}}(X, P_X, Y, P_Y) = \frac{\omega}{2}(P_X^2 + X^2) + \frac{\alpha}{2}(P_Y^2 - Y^2) + \epsilon_s, \tag{14}$$

where ω and α are positive constants. This Hamiltonian has equations of motion

$$\frac{\mathrm{d}}{\mathrm{d}t}\begin{pmatrix} X \\ P_X \\ Y \\ P_Y \end{pmatrix} = \begin{pmatrix} \omega P_X \\ -\omega X \\ \alpha P_Y \\ \alpha Y \end{pmatrix}, \tag{15}$$

which we match with (12) by letting $x = X$ and $y = Y$. This leads to $\omega P_X = p_x/m_x$ and $\alpha P_Y = p_y/m_y$. Matching the time derivatives of these relationships,

$$\frac{\mathrm{d}}{\mathrm{d}t}\omega P_X = -\omega^2 x = \frac{\mathrm{d}}{\mathrm{d}t}\frac{p_x}{m_x} = \frac{-2D_x\lambda^2 x}{m_x} \tag{16}$$

$$\frac{\mathrm{d}}{\mathrm{d}t}\alpha P_Y = \alpha^2 y = \frac{\mathrm{d}}{\mathrm{d}t}\frac{p_y}{m_y} = \frac{4V^\ddagger y/y_w^2}{m_y} \tag{17}$$

$$\implies \omega = \lambda\sqrt{\frac{2D_x}{m_x}}, \quad \alpha = \frac{2}{y_w}\sqrt{\frac{V^\ddagger}{m_y}} \tag{18}$$

2.4 Statisical Mechanical Reaction Flux

Now that we have the linearised system in canonical form, we make use of the result of the calculation made in reference [6] for the flux over an index-one saddle, which we calculate to be

$$\mathcal{F}_E = \frac{2\pi}{\omega}\left(E - \epsilon_s\right) = \frac{\pi}{\lambda}\sqrt{\frac{2m_x}{D_x}}\left(E - \epsilon_s\right). \tag{19}$$

We see that the reaction flux is inversely proportional to the Morse parameter λ, and is inversely proportional to the square root of the dissociation energy D_x. This approximation should hold at an energy level close to that of the saddle.

Another way of calculating the flux, from which the above formula was derived, is described in [7]. Starting from the definition of reaction flux and then applying Stokes' theorem, it can be shown that the flux is the action around the periodic orbit (p.o.)

$$\mathcal{F}_E = \oint_{\text{p.o.}} \mathbf{p}\cdot\mathrm{d}\mathbf{q}. \tag{20}$$

In the case of the De Leon Berne system, this amounts to integrating p_x with respect to x. Refering back to (5), we calculate

$$\mathcal{F}_E = 2\int_{x_{\min}}^{x_{\max}} \sqrt{2m_x D_x\left(\kappa^2 - \left(1 - e^{-\lambda x}\right)^2\right)}\mathrm{d}x \tag{21}$$

$$= \frac{2\sqrt{2m_x D_x}\kappa^2}{\lambda}\int_{-\pi/2}^{\pi/2} \frac{\cos^2\theta}{1 - \kappa\sin\theta}\mathrm{d}\theta \tag{22}$$

where the last equality was obtained through the substitution $1 - \exp(-\lambda x) = \kappa \sin\theta$. Then, if we only consider energy values for which $\epsilon_s \leq E \leq D_x + \epsilon_s$, or equivalently $\kappa \in [0, 1]$, we see that the integral

$$I(\kappa) := \int_{-\pi/2}^{\pi/2} \frac{\cos^2\theta}{1 - \kappa \sin\theta} \mathrm{d}\theta$$

is monotonically increasing in κ attaining values between $\pi/2$ and π. Backfilling κ, we obtain the result

$$\mathcal{F}_E = \frac{2}{\lambda}\sqrt{\frac{2m_x}{D_x}}(E - \epsilon_s)I(\kappa) \approx \frac{\pi}{\lambda}\sqrt{\frac{2m_x}{D_x}}(E - \epsilon_s) \tag{23}$$

where the approximation holds for small κ, and thus aligns with our initial calculation.

2.5 Reaction Gap Times

In this section, we explore the idea of gap time, specifically for the De Leon Berne system. Historically [2] the notion of gap time has been defined in configuration coordinates as the time between sign changes of the reaction coordinate. While this definition is sufficient for simple systems in which the dividing surfaces corresponds to a single curve in configuration space (in this case $y = 0$), we ultimately want to consider a more robust definition that can be applied to any system in which the reaction is defined by the crossing of a dividing surface in phase space, as discussed above [3]. Being surfaces of (local) no-recrossing, the forward and backward dividing surfaces are the surfaces through which a forward or backward reacting trajectory necessarily crosses, respectively [1].

In the De Leon Berne system, the two wells, which correspond to reactant and product states, are identical; the system is symmetric through the reaction coordinate y. Thus, without loss of generality, we consider only the forward dividing surface in this study.

2.5.1 Computating Mean Gap Time

Sampling points uniformly on the forward dividing surface, as described in 2.2.1, we use each point as initial conditions to integrate through the vector field, yeilding a constant-energy ensemble of forward-reacting trajectories. Recording the time taken for each trajectory to backward react (i.e. the time spent in the reactant well), we can obtain a numerical calculation for the average gap time. We repeat this process for a variety of values of the total energy E and values of λ and ζ.

[Note: the gap times were capped at 500 due to the long computation times. Any gap times longer than 500 are recorded as 500, so the mean values calculated will be lower than they should be.]

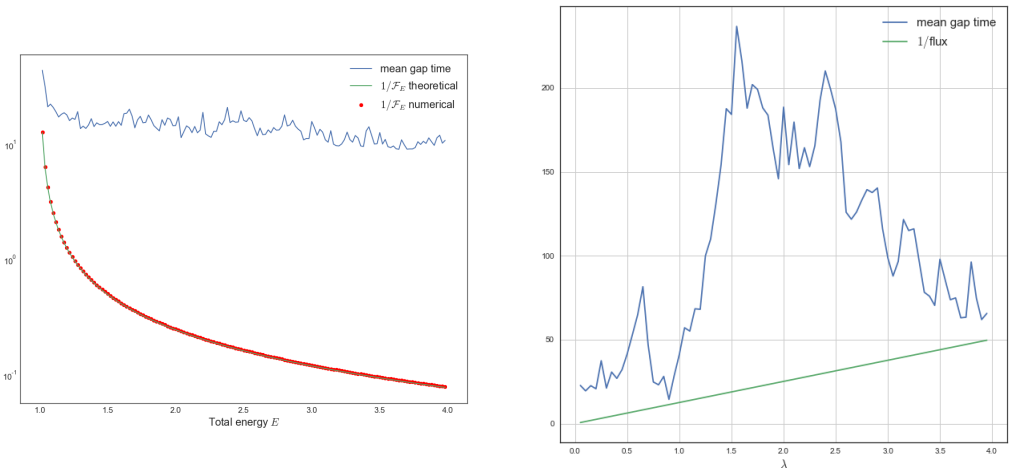

Figure 6: *Left*: Mean gap time against the reciprocal of the flux for varying total energy values, with $\lambda = 1$, $\zeta = 1$. A qualitative relationship between flux and gap time may be inferred here, although further simulations are required for more parameter values. *Right*: Mean gap time and flux caluclation against λ for $\zeta = 1$ and total energy $E = 1.02$. The complicated phase space structures, as can be seen in the Poincaré sections, must be playing a part here, as the behaviour of the gap time with changing λ is clearly a non-linear relationship, despite the flux being inversely proportional to λ.

It would be insightful to repeat these calculations for more values of ζ and E. However the calculation of gap times is computationally intense, so a better optimised way of solving for the gap times would prove fruitful.

2.5.2 Gap Time Distribution over the DS

Another potentially insightful thing to look at is how the initial position on the DS affects the gap time of the resultant trajectory. Figure 7 shows heat maps of the gap times. Each point on the DS is projected onto the (x, p_x) plane, and the gap time for the trajectory that passes through that point is recorded. The results reveal some interesting phase space structures. This method of visualisation may be used in conjunction with the Poincaré sections. Comparing with Figure 3, while similarities are not apparent in general, we can see that for the $\zeta = 0.1$ columns, the ligher coloured edges for the Poincaré sections do seem to correspond to longer gap times in those regions, which explains why there are fewer trajectories passing through those points.

We can also plot histograms of the same calculations, as in Figure 8. We see that for $\lambda = 0.1$, there are very clear peaks of gap times roughly 100 time units apart, while for $\lambda = 2.5$ the gap times are more uniformly distributed beyond a certain point. The vertical dashed lines show the mean gap times. Qualitatively speaking, we may infer an increasing relationship between ζ and the mean gap time, while for λ the story may be more complicated.

In Figure 9, we see very clear peaks for $\lambda = 1.5$ and $\lambda = 3$ while distributions for other values have less clear structures.

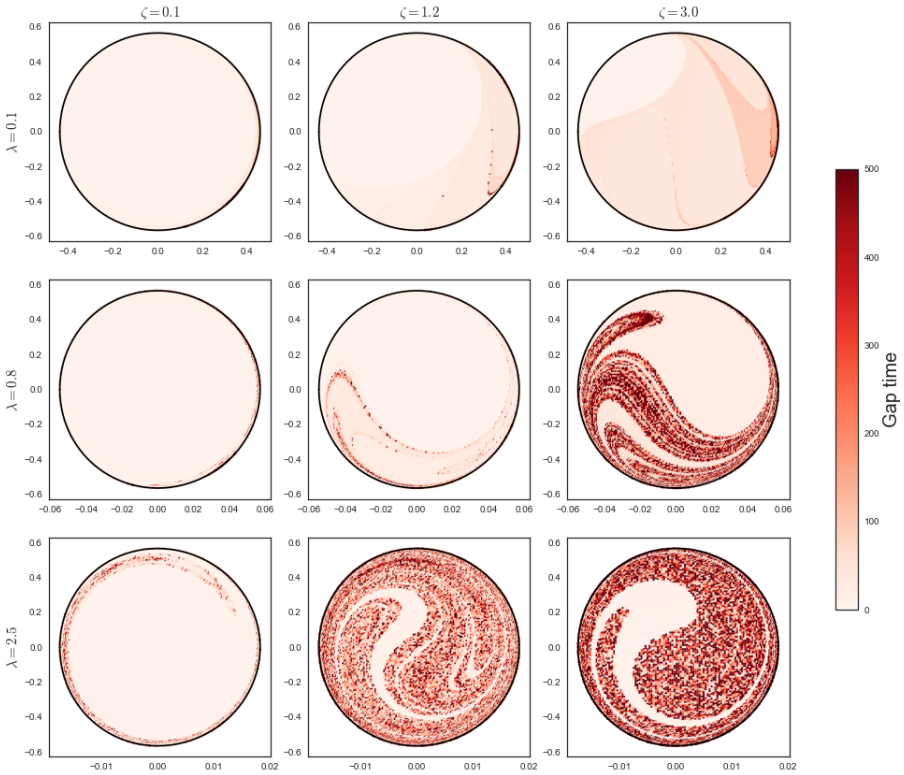

Figure 7: Heat maps showing gap time distribution across the (x, p_x) projection of the DS, $E = 1.02$, λ and ζ varying.

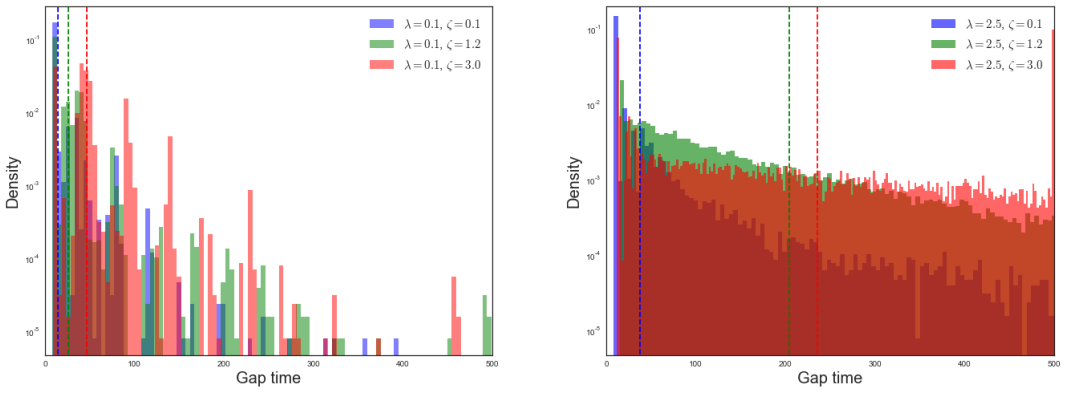

Figure 8: Histograms (note the logarithmic vertical scale) showing distribution of gap times over the DS for varying ζ at two different values of λ and with $E = 1.02$.

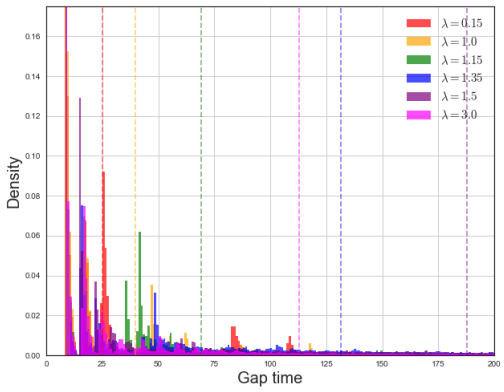

Figure 9: Histogram of gap times for multiple values of λ with $\zeta = 1$, $E = 1.02$. Here a linear vertical axis was more suitable to minimise clutter.

2.6 Complementary Videos

Below are the YouTube links to some animations to go alongside the De Leon Berne system calculations.

- An example trajectory in configuration space, recording gap times: `https://youtu.be/X1Ie-PDKLwY`
- Animated trajectories of points initiated on the forward and backward dividing surfaces integrated through time.
  Total energy $E = 1.02$: `https://youtu.be/1P64W1qhzys`.
  Total energy $E = 2.00$: `https://youtu.be/dQHK7geayR8`

3 The Gezelter-Miller Hamiltonian

In this section, we discuss another two degree-of-freedom Hamiltonian system introduced by Gezelter and Miller [8], which is used as a model for the isomerization of ketene. This system is more complicated, with three potential wells: a well for a reactant state, a product state, and an intermediary well between the two. The energy Hamiltonian again takes the form kinetic plus potential energy:

$$\mathcal{H}(x, y, p_x, p_y) = \frac{p_x^2}{2m_x} + \frac{p_y^2}{2m_y} + V(x, y), \tag{24}$$

where the potential is given by

$$V(x, y) = a_2 x^2 + a_4 x^4 + a_6 x^6 + c x^2 e^{-dx^2} + \frac{1}{2} k \left(y + \frac{d_0}{k} x^4 \right)^2. \tag{25}$$

The parameter values are given by

$$\begin{aligned} a_2 &= -2.3597 \times 10^{-3} \\ a_4 &= 1.0408 \times 10^{-3} \\ a_6 &= -2.7.5496 \times 10^{-4} \\ c &= 7.7569 \times 10^{-3} \\ d &= 1.9769 \\ d_0 &= -2.45182 \times 10^{-4} \\ k &= 1.0074 \times 10^{-2} \end{aligned} \tag{26}$$

and in the studies that follow we will consider varying the mass of the x degree of freedom, $m_x \in \{1, 2, 4, 8, 16, 32, 64 \ldots\}$ with $m_y = 1$.

The equations of motion due to Hamilton's equations are given by

$$\begin{aligned} \dot{x} &= \frac{\partial \mathcal{H}}{\partial p_x} = \frac{p_x}{m_x}, \quad \dot{y} = \frac{\partial \mathcal{H}}{\partial p_y} = \frac{p_y}{m_y} \\ \dot{p_x} &= -\frac{\partial \mathcal{H}}{\partial x} = -2a_2 x - 4a_4 x^3 - 6a_6 x^5 + 2cxe^{-dx^2}\left(1 - dx^2\right) - 4d_0 x^3 \left(y + \frac{d_0}{k} x^4\right) \\ \dot{p_y} &= -\frac{\partial \mathcal{H}}{\partial y} = -k\left(y + \frac{d_0}{k} x^4\right). \end{aligned} \tag{27}$$

Figure 10 shows a heat map of the potential energy surface in configuration space and the positions of the three centre-centre and four centre-saddle equilibrium points, as well as contours, known as separatrices, that correspond to the energy levels of the centre-saddles. The separatrices divide the configuration space into regions only accessible to trajectories with sufficient energy.

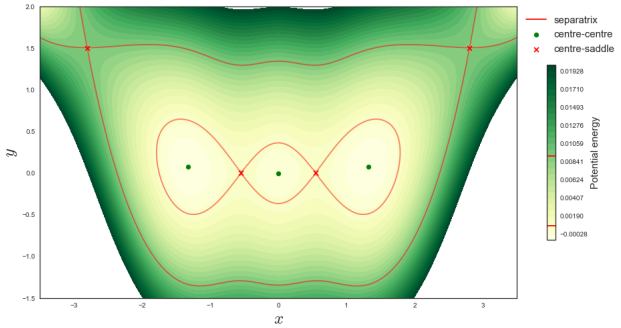

Figure 10: Contour plot for the Gezelter-Miller potential.

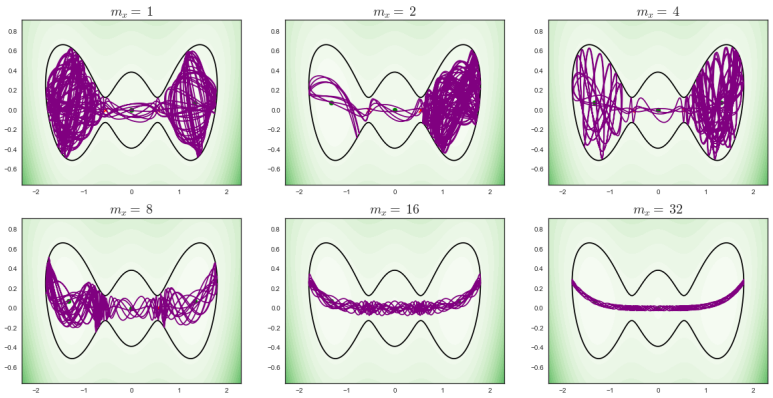

Figure 11: Some example trajectories in configuration space for varying values of m_x. It seems the larger the mass, the smaller the oscillation in the y coordinate.

3.1 Poincaré sections

The first feature we notice after observing some example trajectories are a tendancy for quickly-reacting trajectories (i.e. trajectories that don't linger in a single well but pass through along $y = 0$), there is a distinctive U-shaped manifold. This is promenant in the Poincaré sections for $p_y = 0$, (Figures 12 and 13a), which are essentially plots of the points at which the trajectory turns around in the y coordinate. It turns out there are indeed a collection of stable period orbits along precisely this manifold. Figure 13b shows the orbit for $m_x = 16$ with initial state $(x, y) = (0, -0.01)$, $p_y = 0$ and $p_x > 0$ such that $E = 0.00075$.

Another feature of these $p_y = 0$ sections are the horizontal lines in the central well. These correspond to trajectories that are passing through the central well, oscillating along the stable manifold. The fact that these lines are horizontal tell us that in this region of configuration space, the degrees of freedom are uncoupled, and the y positions of the lines are the amplitude of oscillation for the y-coordinate oscillator. This is because for $|x| \ll 1$, the Hamiltonian may be approximated by that of an uncoupled system featuring a simple harmonic oscillator in the y coordinate.

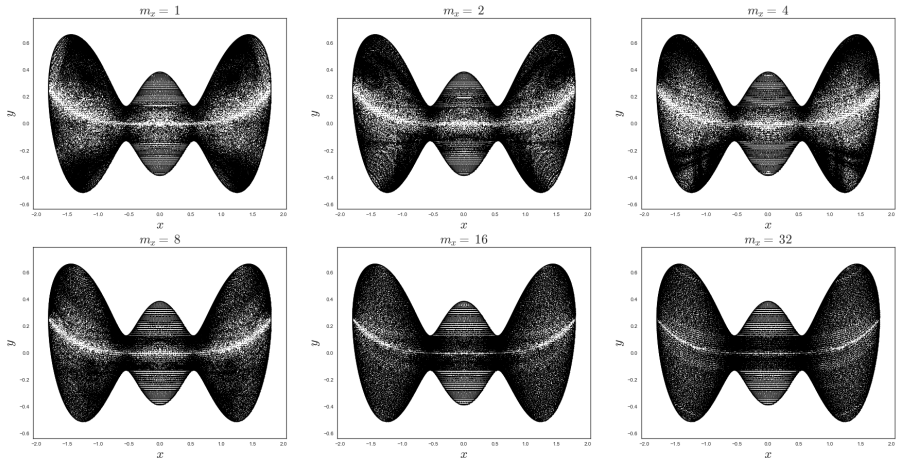

Figure 12: Poincaré sections $p_y = 0$ in configuration space for the Gezelter-Miller potential at various masses, with total energy $E = 0.00075$. The higher the mass, the smaller the minimum amplitude of oscillation in the y coordinate.

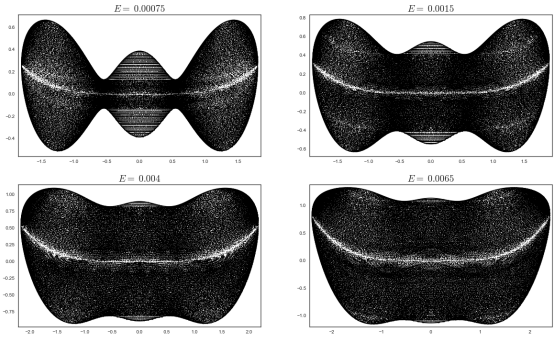

(a) Poincaré sections $p_y = 0$ in configuration space at various energy levels, with $m_x = 16$

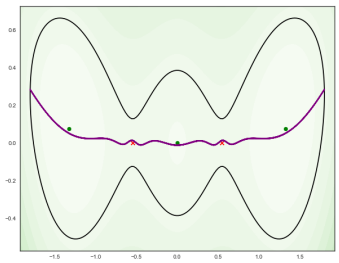

(b) An example of a stable periodic orbit at energy level $E = 0.00075$.

Another interesting Poincaré section is for $p_x = 0$ in configuration space, shown in Figure 14. Each trajectory intersects $p_x = 0$ along two of the lines. Comparing with the stable manifold shown in Figure 13b and the example trajectories shown in Figure 11, we see that the flat part in the middle of the stable manifold corresponds with the vertical lines in the $p_x = 0$ section, while the parts that bend up correspond to the overlapping lines. This suggests that the system behaves as though it is uncoupled along two generalised coordinates oriented tangent and transverse to the stable manifold.

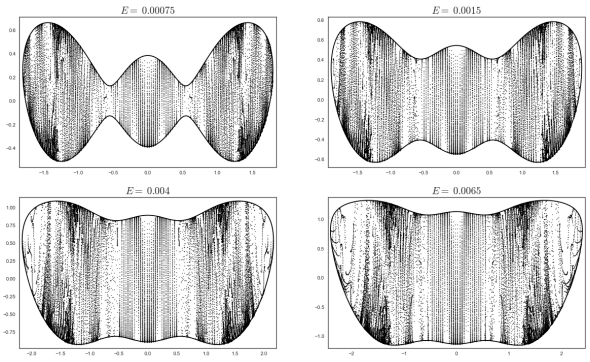

Figure 14: Poincaré sections $p_x = 0$ in configuration space at various energy levels, with $m_x = 16$.

3.2 Direction for further research

The techniques deployed in Section 2 to analyse the De Leon Berne system are very powerful tools in gaining an understanding of these non-linear systems. It'd be insightful to numerically solve for the UPOs in this system and analyse the dividing surfaces around these UPOs to see how mass and energy effects reaction flux and gap times in this model.

References

[1] Wiggins: *The Role of Normally Hyperbolic Invariant Manifolds (NHIMs) in the Context of the Phase Space Setting for Chemical Reaction Dynamics*, 2016 `https://doi.org/10.1134/S1560354716060034`

[2] De Leon, Berne, Rosenberg: *Isomerization Dynamics and the Transition to Chaos*, 1982 `https://doi.org/10.1063/1.442459`

[3] Ezra, Waalkens, Wiggins: *Microcanonical rates, gap times, and phase space dividing surfaces*, 2009, `https://doi.org/10.1063/1.3119365`

[4] Ezra, Wiggins: *Sampling Phase Space Dividing Surfaces Constructed from Normally Hyperbolic Invariant Manifolds (NHIMs)*, 2018, `https://doi.org/10.1021/acs.jpca.8b07205`

[5] Waalkens et. al: *A formula to compute the microcanonical volume of reactive initial conditions in transition state theory*, 2005, `https://doi.org/10.1088/0305-4470/38/45/L03`

[6] R.S Mackay: *Flux over a saddle*, 1990 `https://doi.org/10.1016/0375-9601(90)90306-9`

[7] Waalkens, Wiggins: *Direct Construction of a Dividing Surface of Minimal Flux for Multi-Degree-of-Freedom Systems: The Equivalence of Conventional and Variational Transition State Theory*, 2004 `arXiv:nlin/0404002`

[8] Mauguière, Collins, Ezra, Farantos, Wiggins, *Roaming dynamics in ketene isomerization*, 2014 `https://doi.org/10.1007/s00214-014-1507-4`